medRxiv preprint doi: https://doi.org/10.1101/2022.11.01.22281820; this version posted November 2, 2022. The copyright holder for this preprint (which was not certified by peer review) is the author/funder, who has granted medRxiv a license to display the preprint in perpetuity. All rights reserved. No reuse allowed without permission.

Integrative analyses of neuroimaging, clinical, and multi-omics data identified meaningful Alzheimer's disease progression subtypes

Qiyuan An, [1], Mengliang Zhang, [2], Xinyue Hu, [3], Chang Su, [4], Yingying Zhu, [5]

[1] Department of Computer Science and Engineering, University of Texas at Arlington [2] Department of Health Services Administration and Policy, Temple University

Abstract:

Alzheimer's Disease (AD) is a common neurodegenerative disorder with diverse clinical manifestations. To better understand differences between diverse manifestations, we investigate from the difference in MRI ROI volumes among subtypes to their related different gene pathways. In this study, we identify three subtypes of AD development with fast, moderate, and slow progression rates from the MRI ROI volume biomarkers in the ADNI cohort. We further find differentially expressed proteins in CSF fluids among these AD patients and related significantly different genetic pathways. A total of 159 patients' data are included for analysis. We identify three distinct subtypes from the hierarchical clustering on MRI ROI volume biomarkers. Subtype 1, characterized as fast progression, consists of 34 patients (21.9%). Subtype 2, as moderate progression, comprises 77 patients (49.6%). Subtype 3, as slow progression, consists of 44 patients (28.3%). These subtypes show significantly differences in cognitive test scores and corresponding genetic pathways.

Keywords:

1 Introduction

Alzheimer's Disease (AD) is a complex and prevalent neurodegenerative disease, whose etiology remains unclear to date. It's heterogeneous in distinct clinical manifestations, progression trajectories, volume biomarker readouts, and genetic pathways. Due to its irreversible and age-related characters and lack of any cure, early diagnosis and intervention of AD deterioration play an significant role in designing clinical treatment strategies. One major challenge for AD prediction and customized clinical treatment is to identify the phenotypic heterogeneity within the AD population [i].

Distinguishing subtypes in AD may lead to insights of different etiological mechanisms, better the customized treatments, and interfere the development of brain atrophy and dementia. The motivation of this study is to investigate into the progression patterns of brain region volume biomarkers among different participants in ADNI cohort, to reveal the underlying atrophy development patterns among different subtypes. We cluster the participant features and identify three subtypes with distinct AD progression patterns in

[1] qxa5560@mavs.uta.edu
[2] mxz3935@mavs.uta.edu
[3] xxh4034@mavs.uta.edu
[4] su.chang@temple.edu
[5] yingying.zhu@uta.edu

NOTE: This preprint reports new research that has not been certified by peer review and should not be used to guide clinical practice.

medRxiv preprint doi: https://doi.org/10.1101/2022.11.01.22281820; this version posted November 2, 2022. The copyright holder for this preprint (which was not certified by peer review) is the author/funder, who has granted medRxiv a license to display the preprint in perpetuity. All rights reserved. No reuse allowed without permission.

the ADNI cohort: subtype 1, fast symptom progression; subtype 2, moderate symptom progression; and subtype 3, slow symptom progression.

Some previous attempts about neurodegenerative disease subtyping can be categorized into the following categories: using neuroimaging biomarkes' readouts to identify distinct patterns of atrophy regions[ii iii], using cognitive test scores[iv v], and using proteomics data[vi vii]. However, none of these works take advantage of all these features and derive the underlying significant genetic pathways.

To this end, we propose to identify subtypes of AD via the neuroimaging biomarkers, find differentially expressed proteins from Cerebrospinal Fluid (CSF) proteomics data, and perform pathway enrichment analysis on omics data to derive significant gene pathways. We hope this study can provide insights to discover individually customized treatment for AD patients.

2 Experiments

2.1 Data Preprocessing

We adopt the ADNI TADPOLE challenge dataset[viii] for our experiment. The TADPOLE standard dataset includes the following biomarkers:

Main cognitive tests – neuropsychological tests administered by a clinical expert:

- CDR Sum of Boxes
- ADAS 11
- ADAS 13
- MMSE
- RAVLT
- MOCA
- Ecog

MRI ROIs (Freesurfer) - measures of brain structural integrity:

- Volumes
- Cortical thicknesses
- Surface areas

We only adopt the MRI ROI volumes as inputs for subtyping, while using cognitive tests to validate the subtyping results. The number of MRI ROI volumes is 270. The TADPOLE dataset includes 1610 participants, which consists of 342 AD, 417 CN, and 872 MCI. Out of 342 AD participants, we filter out participants with less than 12 months longitudinal data and result in 313 participants. After that, we build each participant's speed feature defined as $\frac{lastvisit - firstvisit}{timeinterval}$, representing the progression rates of different ROI volumes. Then we filter the speed feature matrix in both the participants and the ROI volume dimensions if the missing rate is greater than 0.7. Filtering speed features

medRxiv preprint doi: https://doi.org/10.1101/2022.11.01.22281820; this version posted November 2, 2022. The copyright holder for this preprint (which was not certified by peer review) is the author/funder, who has granted medRxiv a license to display the preprint in perpetuity. All rights reserved. No reuse allowed without permission.

results in 239 columns ROI volumes and 159 participants. In the end, we perform minmax normalization on the speed feature matrix.

2.2 Matrix Decomposition

We decompose the speed matrix via Truncated SVD with rank of 3 to derive participants' features. The choice of Truncated SVD is for its native suitability for sparse matrix as our speed feature matrix has many missing values. The actual implementation of decomposition is via the sklearn library[ix].

2.3 Clustering

Then we cluster decomposed participants' features via the hierarchical clustering to avoid the biased/wrong prior hypothesis of number of subtypes. Our clustering results in 3 phenotypes (number of participants) that correspond to fast progression (34), moderate progression (44), and mild progression (77). We validate the subtyping results on cognitive test scores shown in Fig 1.

medRxiv preprint doi: https://doi.org/10.1101/2022.11.01.22281820; this version posted November 2, 2022. The copyright holder for this preprint (which was not certified by peer review) is the author/funder, who has granted medRxiv a license to display the preprint in perpetuity. All rights reserved. No reuse allowed without permission.

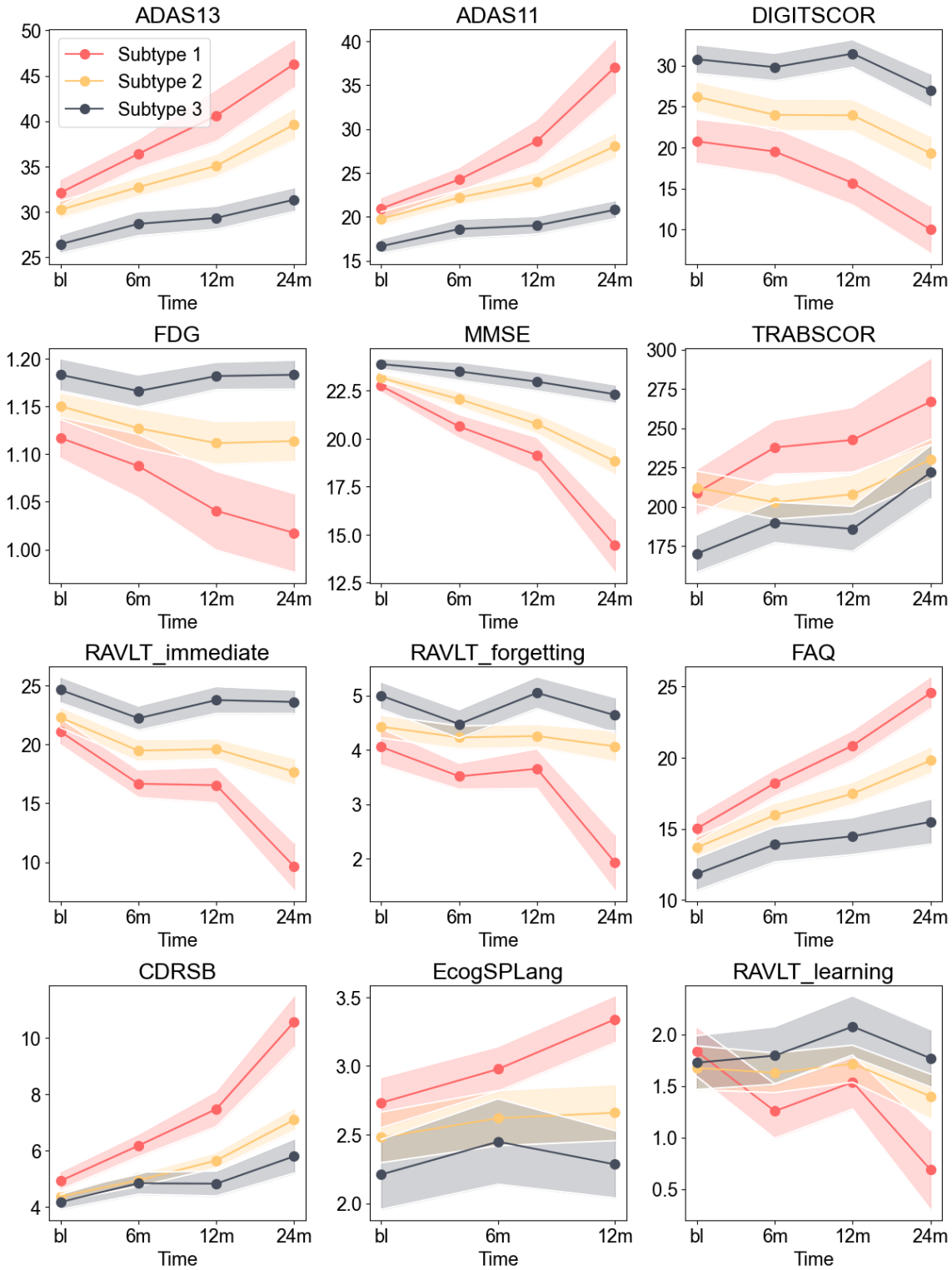

Figure 1. Cognitive test scores in 3 subtypes. Red: subtype 1, yellow: subtype 2, gray: subtype 3.

Each strip in Fig 1 represents the longitudinal trend on one cognitive test of one subtype.

medRxiv preprint doi: https://doi.org/10.1101/2022.11.01.22281820; this version posted November 2, 2022. The copyright holder for this preprint (which was not certified by peer review) is the author/funder, who has granted medRxiv a license to display the preprint in perpetuity. All rights reserved. No reuse allowed without permission.

The solid line in the center is the mean of the cognitive test, while the light color between the solid line is the standard error. The clear separability of cognitive scores justifies the legitimacy of our method on different progression trends.

2.4 Significance test on ROI volumes

We perform the Kruskal-Wallis test among ROI volumes under different subtypes and below Table 1 and Fig. 2 show significant ROI volumes. The choice of Kruskal-Wallis rather than the ANOVA test is because distributions of ROI volumes are not normal distribution.

FLDNAME	P-values
Volume (Cortical Parcellation) of LeftPrecentral	0.00378
Volume (Cortical Parcellation) of RightLateralOrbitofrontal	0.004316
Volume (WM Parcellation) of LeftInferiorLateralVentricle	0.005641
Volume (Cortical Parcellation) of RightPrecentral	0.008466
Volume (Cortical Parcellation) of LeftParacentral	0.011357
Volume (Cortical Parcellation) of LeftPrecentral	0.014085
Volume (WM Parcellation) of LeftVessel	0.017018
Volume (WM Parcellation) of LeftInferiorLateralVentricle	0.019348
Volume (Cortical Parcellation) of LeftParacentral	0.020999
Volume (WM Parcellation) of RightInferiorLateralVentricle	0.025208
Volume (Cortical Parcellation) of LeftFrontalPole	0.026786
Volume (Cortical Parcellation) of RightPrecentral	0.030398
Volume (WM Parcellation) of LeftLateralVentricle	0.031343
Volume (Cortical Parcellation) of LeftPostcentral	0.033126
Volume (Cortical Parcellation) of RightTemporalPole	0.033798
Volume (WM Parcellation) of LeftLateralVentricle	0.035684
Volume (Cortical Parcellation) of RightTransverseTemporal	0.048881

Table 1: Significant ROI volumes and p-values

medRxiv preprint doi: https://doi.org/10.1101/2022.11.01.22281820; this version posted November 2, 2022. The copyright holder for this preprint (which was not certified by peer review) is the author/funder, who has granted medRxiv a license to display the preprint in perpetuity. All rights reserved. No reuse allowed without permission.

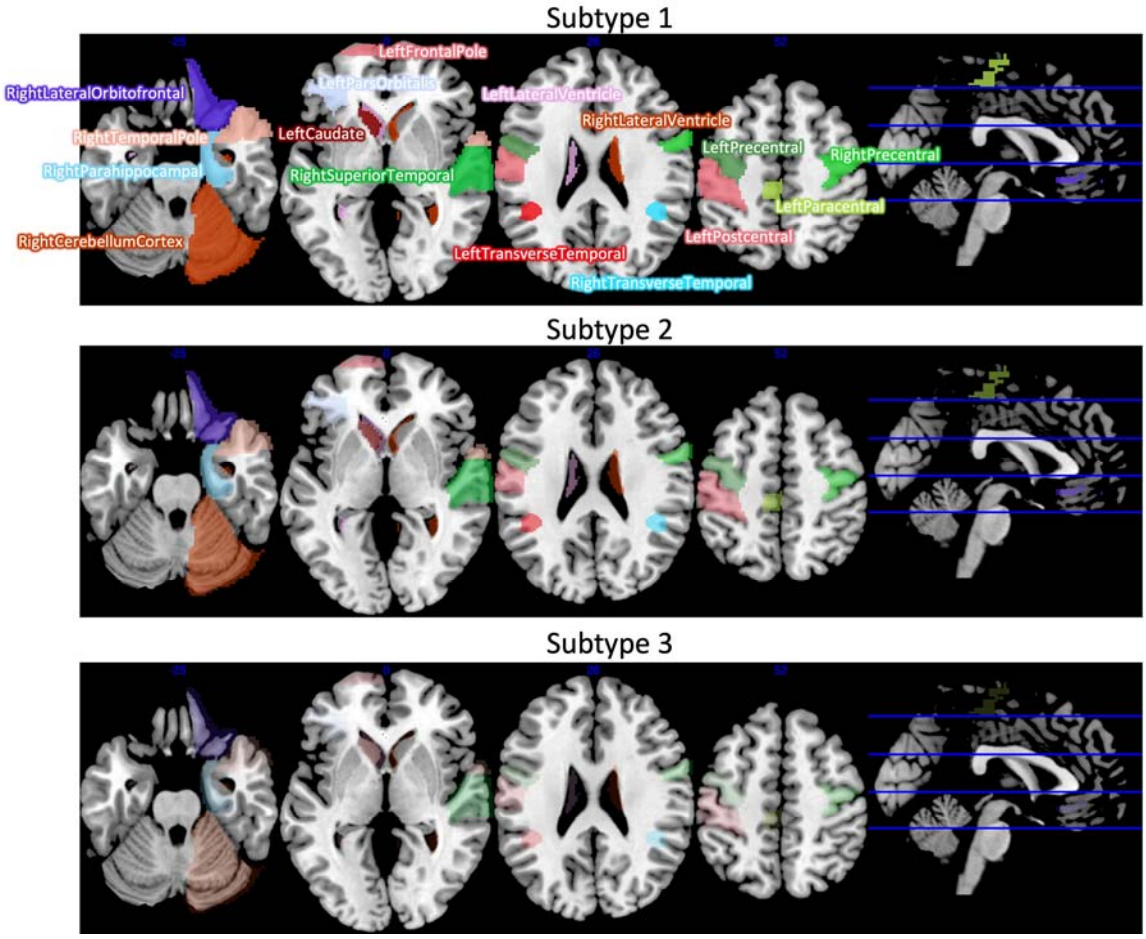

Figure 2. Significant ROI biomarkers

2.5 Find significant proteins from subtyping

We use ADNI's Biomarkers Consortium CSF Proteomics MRM dataset (CSFMRM) to find significantly different proteins between each subtype and normal control (CN) group. The intersected number of participants between 3 subtypes and the CSFMRM are subtype 1 has 10, subtype 2 has 13, and subtype 3 has 20 respectively. While the number of CN participants between the TADPOLE dataset and CSF proteomics is 86.

We first build a contrast matrix between each pair of subtype and CN conditioned on age, gender, and year of education factors to eliminate the bias introduced by these factors. Then we fit a linear model for each pair of subtype and CN and find significant proteins by thresholding $|\log FC| > 0.2$ and $Padj < 0.05$ from the empirical Bayes's statistical tests. The p-value (Padj) is corrected by FDR. The actual implementation is via limma library in R. The resulted significant proteins are in Table 2.

Subtype 1	Subtype 2	Subtype 3
NPTXR	NPTXR	FABPH
NPTX2	FABPH	NPTXR
VGF	PIMT	PIMT

medRxiv preprint doi: https://doi.org/10.1101/2022.11.01.22281820; this version posted November 2, 2022. The copyright holder for this preprint (which was not certified by peer review) is the author/funder, who has granted medRxiv a license to display the preprint in perpetuity. All rights reserved. No reuse allowed without permission.

CA2D1	KLK11	GFAP
AMD	SCG3	PCSK1
PTPRN	CH3L1	
NPTX1	GFAP	
NRX1A	NPTX1	
NRX3A	MUC18	
NRX2A		
CCKN		
NELL2		
CAD13		
SCG2		
NRCAM		
PDYN		
PCSK1		
NEGR1		
NCAN		
FAM3C		
PLDX1		
SE6L1		
CD59		
CSTN1		
CNTN1		
PIMT		
CMGA		
FABPH		
SCG3		
MUC18		
TNR21		
NEO1		
L1CAM		
B3GN1		
BTD		
NBL1		
SPRL1		
NCAM1		
PVRL1		
CADM3		

Table 2: Significant proteins between subtypes and CN.

2.6 Find significant pathways from proteins

After we obtain the significant proteins between each pair of subtype and CN, we adopt

medRxiv preprint doi: https://doi.org/10.1101/2022.11.01.22281820; this version posted November 2, 2022. The copyright holder for this preprint (which was not certified by peer review) is the author/funder, who has granted medRxiv a license to display the preprint in perpetuity. All rights reserved. No reuse allowed without permission.

g:profiler[x] to perform pathway enrichment analysis and determine statistically enriched gene pathways. We correct p-value of 0.05 threshold with the Benjamini-Hochberg FDR. The gene data sources are GO molecular function, GO cellular component, GO biological process, KEGG, and Reactome. Then we filter output significant pathways by limiting term size between 5 and 350. The resulted pathways between each subtype and CN are listed in Fig 3.

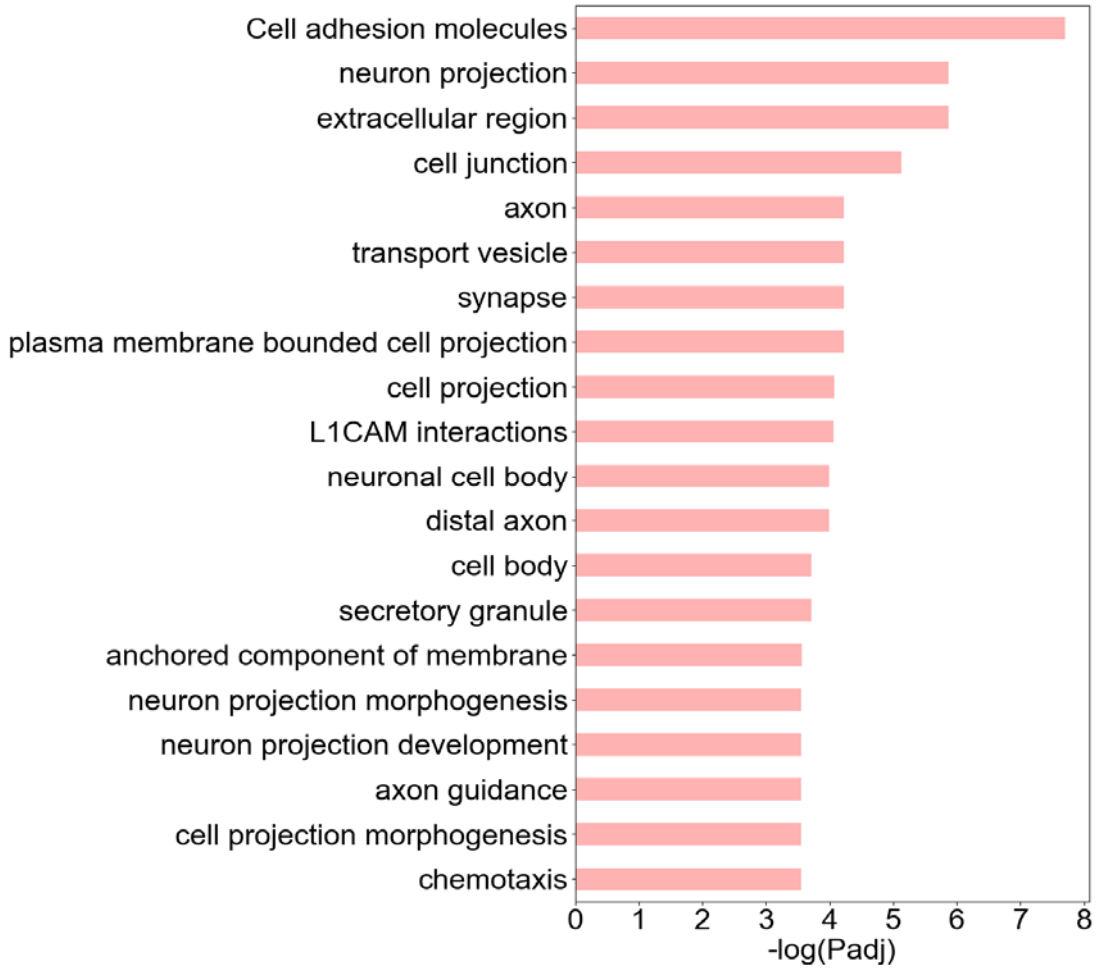

medRxiv preprint doi: https://doi.org/10.1101/2022.11.01.22281820; this version posted November 2, 2022. The copyright holder for this preprint (which was not certified by peer review) is the author/funder, who has granted medRxiv a license to display the preprint in perpetuity. All rights reserved. No reuse allowed without permission.

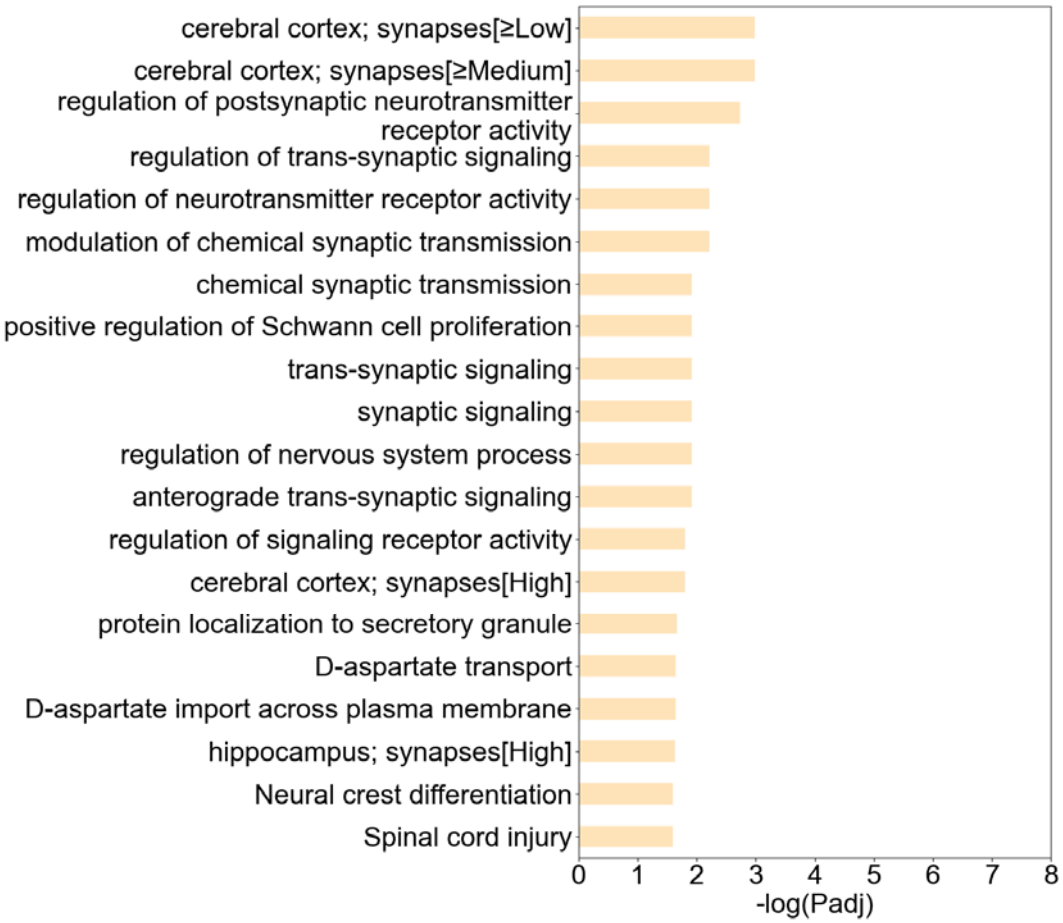

medRxiv preprint doi: https://doi.org/10.1101/2022.11.01.22281820; this version posted November 2, 2022. The copyright holder for this preprint (which was not certified by peer review) is the author/funder, who has granted medRxiv a license to display the preprint in perpetuity. All rights reserved. No reuse allowed without permission.

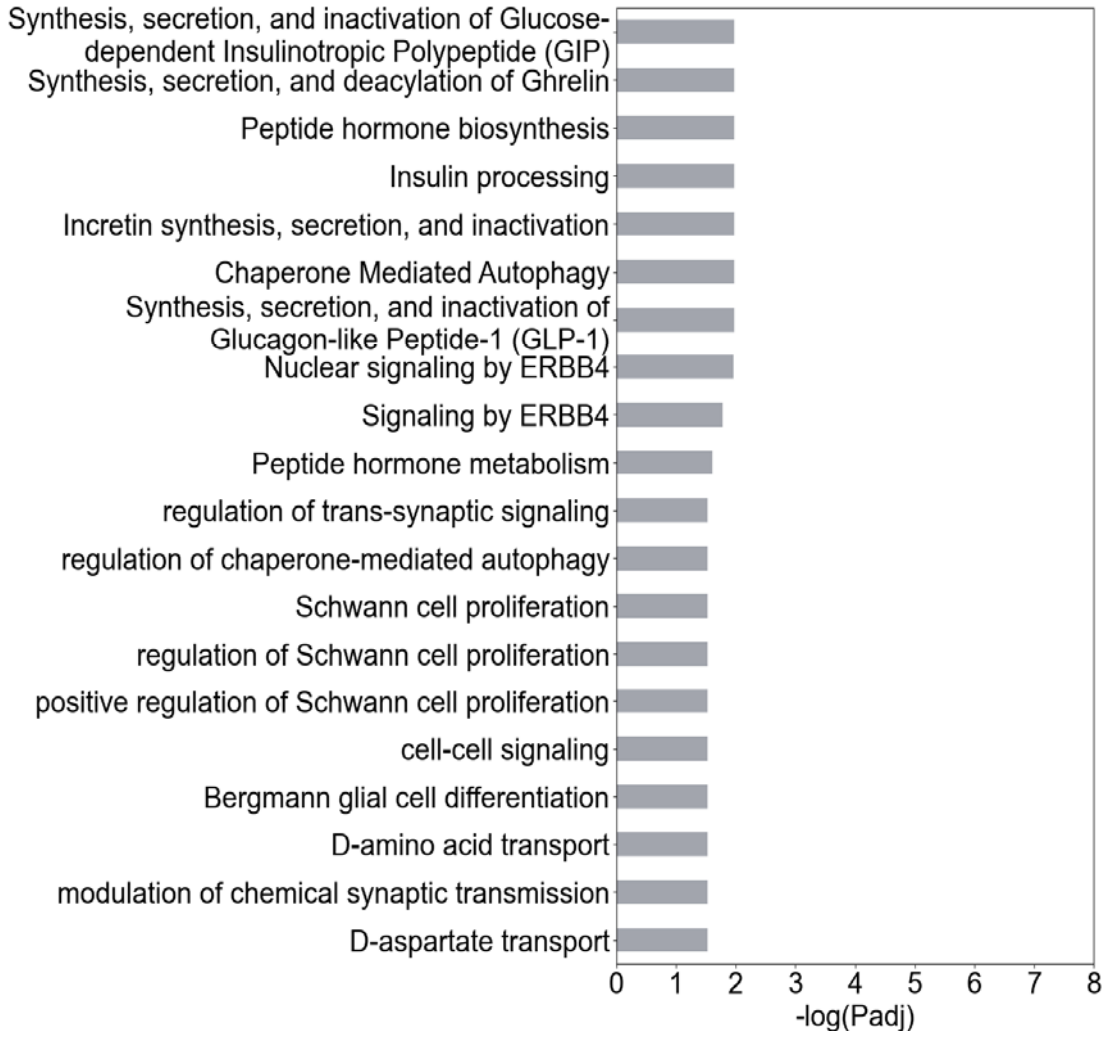

Figure 3. Genetic pathways in 3 subtypes. Red: subtype 1, yellow: subtype 2, gray: subtype 3.

References

[i] Satone et al., "Learning the Progression and Clinical Subtypes of Alzheimer's Disease from Longitudinal Clinical Data."

[ii] Ferreira et al., "Distinct Subtypes of Alzheimer's Disease Based on Patterns of Brain Atrophy: Longitudinal Trajectories and Clinical Applications."

[iii] Goyal et al., "Characterizing Heterogeneity in the Progression of Alzheimer's Disease Using Longitudinal Clinical and Neuroimaging Biomarkers"; Su et al., "Comprehensively Modeling Heterogeneous Symptom Progression for Parkinson's Disease Subtyping."

[iv] Faghri et al., "Identification and Prediction of Parkinson's Disease Subtypes and Progression Using

medRxiv preprint doi: https://doi.org/10.1101/2022.11.01.22281820; this version posted November 2, 2022. The copyright holder for this preprint (which was not certified by peer review) is the author/funder, who has granted medRxiv a license to display the preprint in perpetuity. All rights reserved. No reuse allowed without permission.

Machine Learning in Two Cohorts."

[v] Satone et al., "Predicting Alzheimer's Disease Progression Trajectory and Clinical Subtypes Using Machine Learning"; Brendel et al., "Comprehensive Subtyping of Parkinson's Disease Patients with Similarity Fusion: A Case Study with BioFIND Data."

[vi] Budgeon et al., "Constructing Longitudinal Disease Progression Curves Using Sparse, Short-Term Individual Data with an Application to Alzheimer's Disease"; Faghri et al., "Identification and Prediction of Parkinson's Disease Subtypes and Progression Using Machine Learning in Two Cohorts."

[vii] Tijms et al., "Pathophysiological Subtypes of Alzheimer's Disease Based on Cerebrospinal Fluid Proteomics."

[viii] Marinescu et al., "Tadpole Challenge: Prediction of Longitudinal Evolution in Alzheimer's Disease."

[ix] Pedregosa et al., "Scikit-Learn: Machine Learning in Python."

[x] Reimand et al., "Pathway Enrichment Analysis and Visualization of Omics Data Using g: Profiler, GSEA, Cytoscape and EnrichmentMap."

Subtype 1

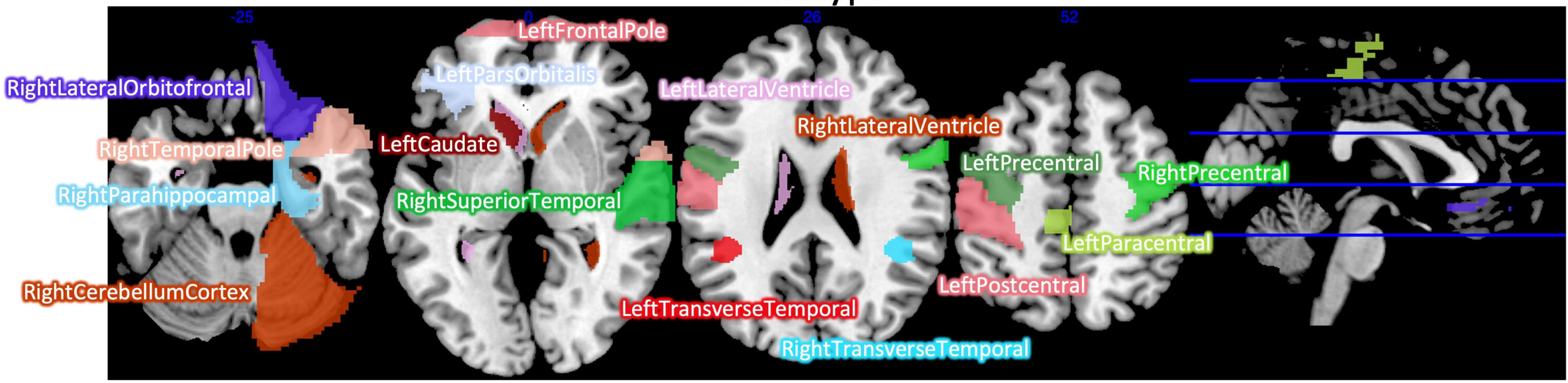

Subtype 2

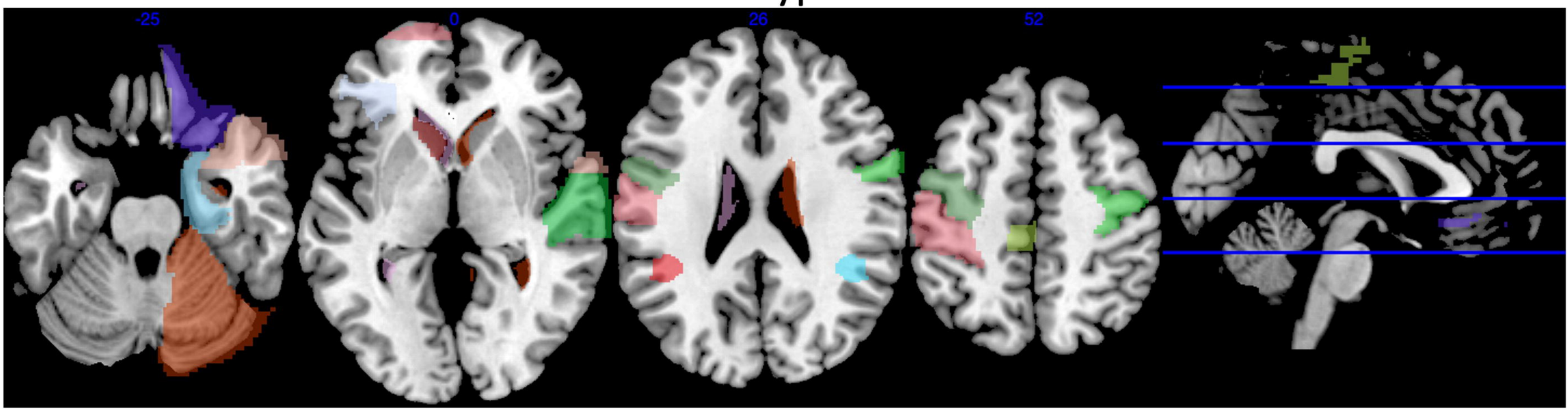

medRxiv preprint doi: https://doi.org/10.1101/2022.11.01.22281820; this version posted November 2, 2022. The copyright holder for this preprint (which was not certified by peer review) is the author/funder, who has granted medRxiv a license to display the preprint in perpetuity. All rights reserved. No reuse allowed without permission.

Subtype 3

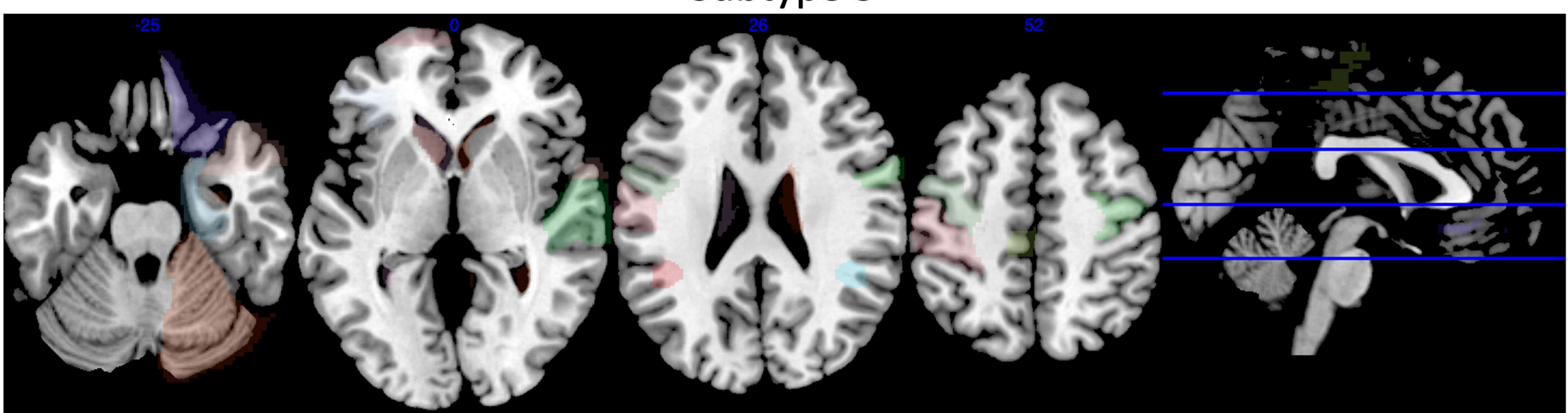

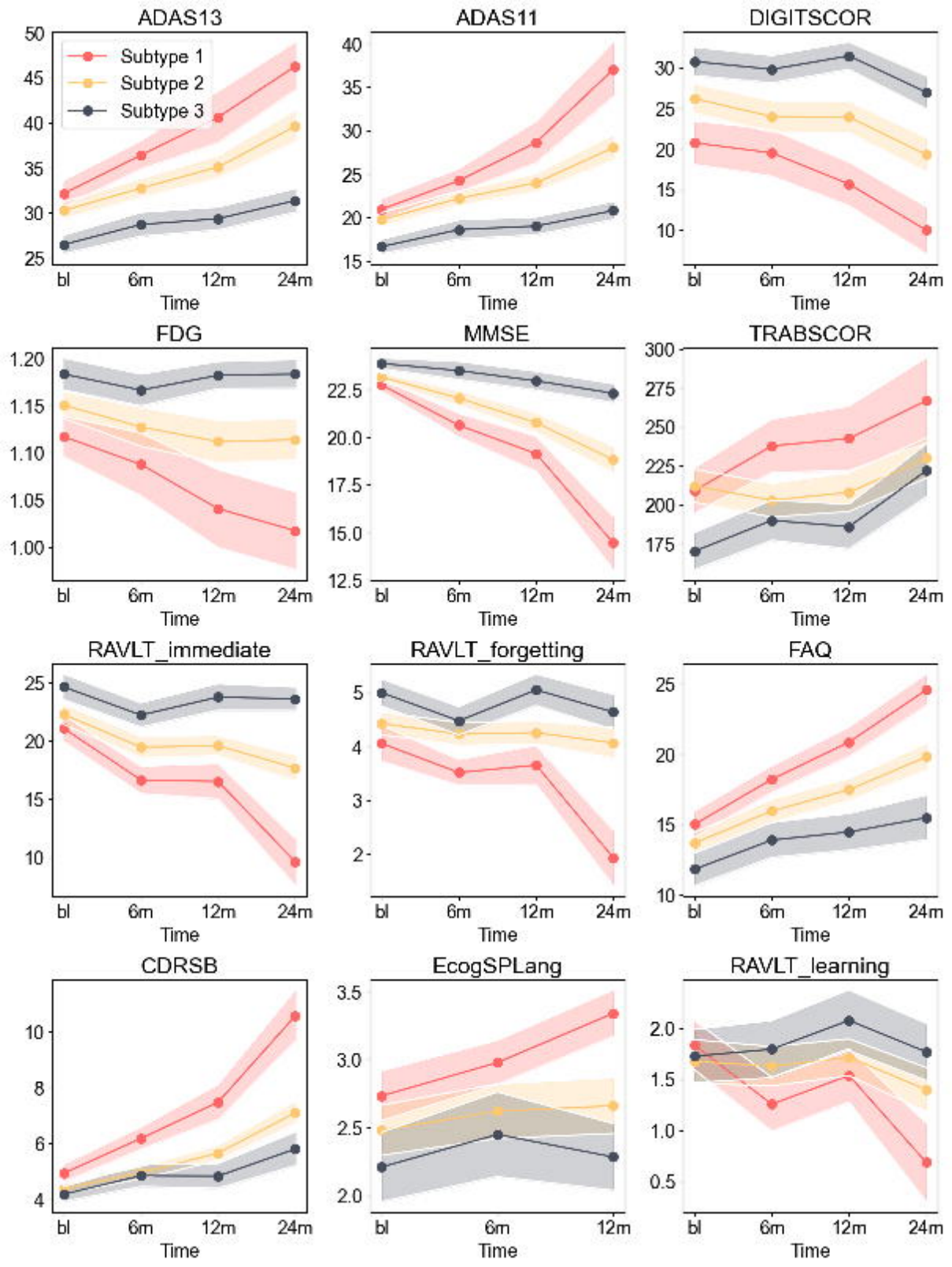
ADAS13
Subtype 1
Subtype 2
Subtype 3
ADAS11
DIGITSCOR
FDG
MMSE
TRABSCOR
RAVLT_immediate
RAVLT_forgetting
FAQ
CDRSB
EcogSPLang
RAVLT_learning
bl
6m
12m
24m
Time

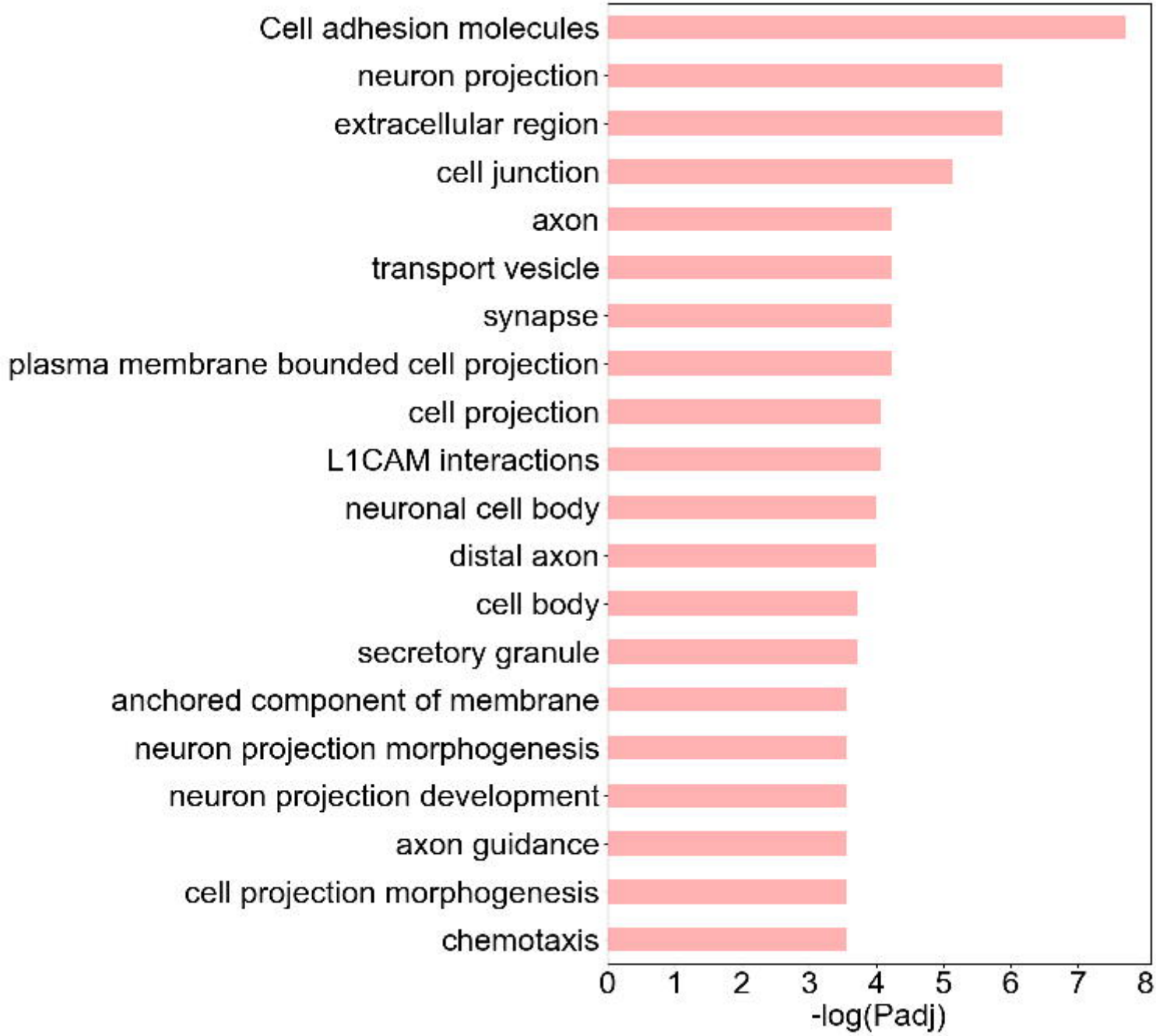
Cell adhesion molecules
neuron projection
extracellular region
cell junction
axon
transport vesicle
synapse
plasma membrane bounded cell projection
cell projection
L1CAM interactions
neuronal cell body
distal axon
cell body
secretory granule
anchored component of membrane
neuron projection morphogenesis
neuron projection development
axon guidance
cell projection morphogenesis
chemotaxis
0
1
2
3
4
5
6
7
8
-log(Padj)

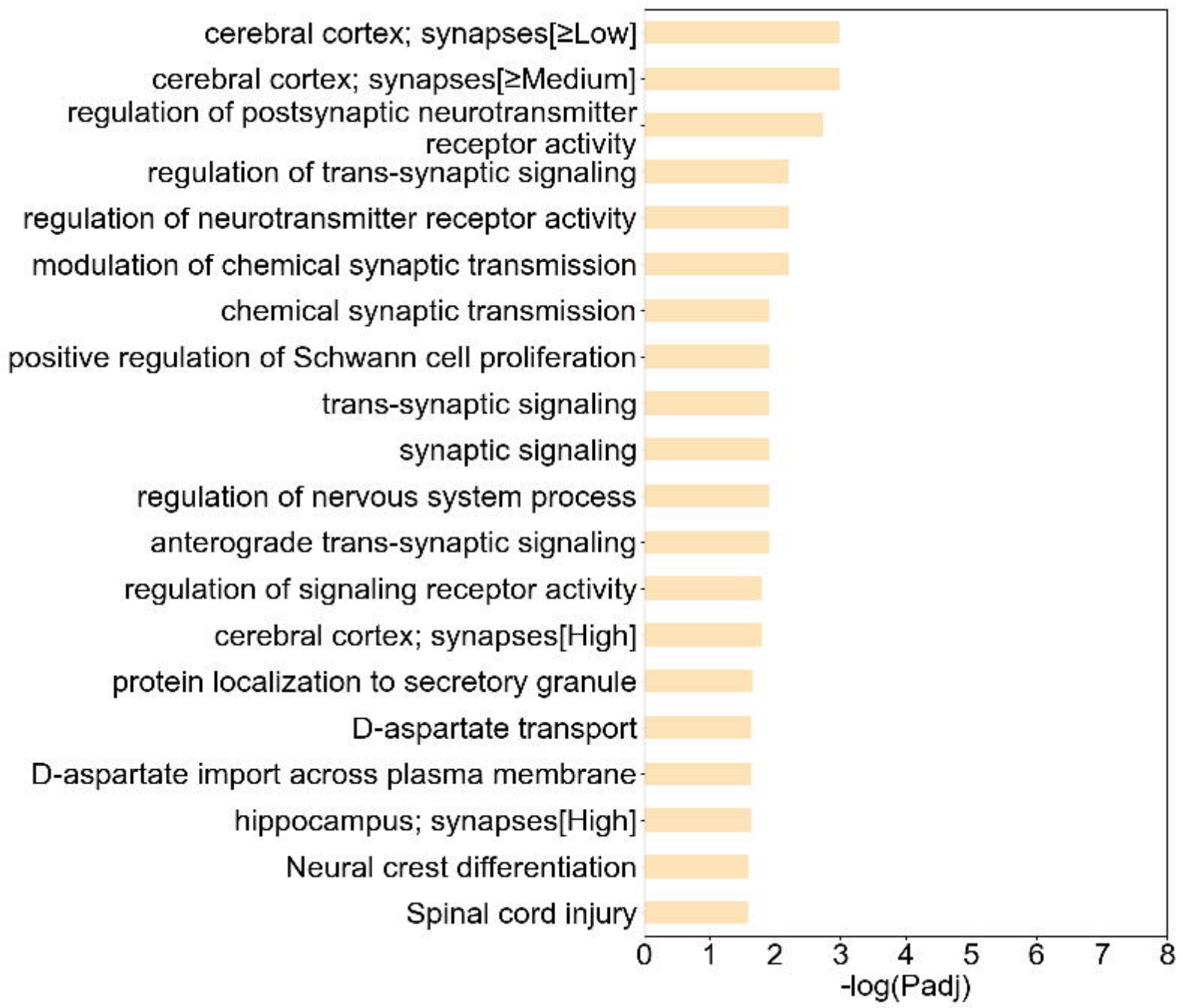
cerebral cortex; synapses[≥Low]
cerebral cortex; synapses[≥Medium]
regulation of postsynaptic neurotransmitter receptor activity
regulation of trans-synaptic signaling
regulation of neurotransmitter receptor activity
modulation of chemical synaptic transmission
chemical synaptic transmission
positive regulation of Schwann cell proliferation
trans-synaptic signaling
synaptic signaling
regulation of nervous system process
anterograde trans-synaptic signaling
regulation of signaling receptor activity
cerebral cortex; synapses[High]
protein localization to secretory granule
D-aspartate transport
D-aspartate import across plasma membrane
hippocampus; synapses[High]
Neural crest differentiation
Spinal cord injury
0
1
2
3
4
5
6
7
8
-log(Padj)

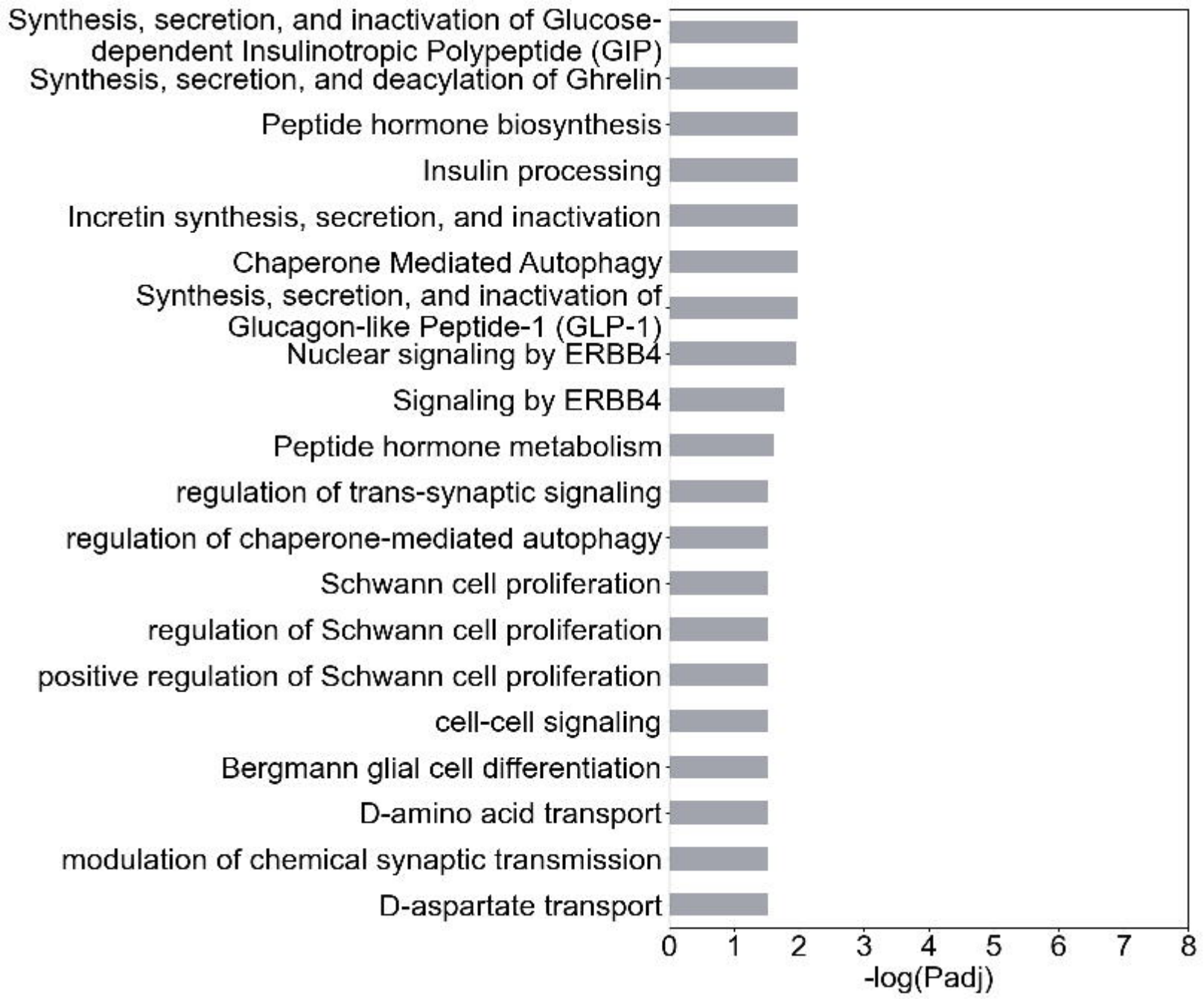
Synthesis, secretion, and inactivation of Glucose-dependent Insulinotropic Polypeptide (GIP)
Synthesis, secretion, and deacylation of Ghrelin
Peptide hormone biosynthesis
Insulin processing
Incretin synthesis, secretion, and inactivation
Chaperone Mediated Autophagy
Synthesis, secretion, and inactivation of Glucagon-like Peptide-1 (GLP-1)
Nuclear signaling by ERBB4
Signaling by ERBB4
Peptide hormone metabolism
regulation of trans-synaptic signaling
regulation of chaperone-mediated autophagy
Schwann cell proliferation
regulation of Schwann cell proliferation
positive regulation of Schwann cell proliferation
cell-cell signaling
Bergmann glial cell differentiation
D-amino acid transport
modulation of chemical synaptic transmission
D-aspartate transport
0
1
2
3
4
5
6
7
8
-log(Padj)